4-2015

Further Insights into the Reaction Be14(CH2,X)10He

M. D. Jones
Michigan State University

Z. Kohley
Michigan State University

T. Baumann
Michigan State University

See next page for additional authors

M. D. Jones, Z. Kohley, T. Baumann, G. Christian, P. A. DeYoung, J. E. Finck, N. Frank, R. A. Haring-Kaye, A. N. Kuchera, B. Luther, S. Mosby, J. K. Smith, J. Snyder, A. Spyrou, S. L. Stephenson, and M. Thoennessen. "Further Insights into the Reaction 14Be(CH2,X)10He." Physical Review C 91.4 (April 2015), 044312.

Further Insights into the Reaction Be14(CH2,X)10He

Abstract

A previously published measurement of the reaction of a 59 MeV/nucleon 14Be beam on a deuterated polyethylene target was further analyzed to search for 12He as well as initial state effects in the population of the 10He ground state. No evidence for either was found. A lower limit of about 1 MeV was determined for a possible resonance in 12He. In addition, the three-body decay energy spectrum of 10He could not be described by a reaction mechanism calculation based on the halo structure of the initial 14Be assuming a direct α-particle removal reaction.

Authors

M. D. Jones, Z. Kohley, T. Baumann, G. Christian, P. A. DeYoung, J. E. Finck, N. Frank, R. A. Haring-Kaye, A. N. Kuchera, B. Luther, S. Mosby, J. K. Smith, J. Snyder, A. Spyrou, Sharon L. Stephenson, and M. Thoennessen

Further insights into the reaction ^{14}Be(CH_2,X)^{10}He

M. D. Jones,[1,2,*] Z. Kohley,[1,3] T. Baumann,[1] G. Christian,[1,2,†] P. A. DeYoung,[4] J. E. Finck,[5] N. Frank,[6] R. A. Haring-Kaye,[7] A. N. Kuchera,[1] B. Luther,[8] S. Mosby,[1,2,‡] J. K. Smith,[1,2,†] J. Snyder,[1,2] A. Spyrou,[1,2] S. L. Stephenson,[9] and M. Thoennessen[1,2]

[1]*National Superconducting Cyclotron Laboratory, Michigan State University, East Lansing, Michigan 48824, USA*
[2]*Department of Physics and Astronomy, Michigan State University, East Lansing, Michigan 48824, USA*
[3]*Department of Chemistry, Michigan State University, East Lansing, Michigan 48824, USA*
[4]*Department of Physics, Hope College, Holland, Michigan 49422-9000, USA*
[5]*Department of Physics, Central Michigan University, Mount Pleasant, Michigan 48859, USA*
[6]*Department of Physics and Astronomy, Augustana College, Rock Island, Illinois 61201, USA*
[7]*Department of Physics and Astronomy, Ohio Wesleyan University, Delaware, Ohio 43015, USA*
[8]*Department of Physics, Concordia College, Moorhead, Minnesota 56562, USA*
[9]*Department of Physics, Gettysburg College, Gettysburg, Pennsylvania 17325, USA*

(Received 11 December 2014; revised manuscript received 27 January 2015; published 15 April 2015)

A previously published measurement of the reaction of a 59 MeV/nucleon ^{14}Be beam on a deuterated polyethylene target was further analyzed to search for ^{12}He as well as initial state effects in the population of the ^{10}He ground state. No evidence for either was found. A lower limit of about 1 MeV was determined for a possible resonance in ^{12}He. In addition, the three-body decay energy spectrum of ^{10}He could not be described by a reaction mechanism calculation based on the halo structure of the initial ^{14}Be assuming a direct α-particle removal reaction.

DOI: 10.1103/PhysRevC.91.044312 PACS number(s): 21.10.Dr, 25.60.−t, 27.20.+n, 29.30.Hs

I. INTRODUCTION

Our recent measurement of the ^{10}He ground state [1] did not support the theoretical explanation for the difference in resonance energy observed in two types of reactions [2]. While a missing mass measurement at Dubna using a (t,p) reaction had reported the ground state to be at 2.1(2) MeV [3], a one-proton removal reaction at GSI from a high-energy ^{11}Li beam found the ground state to be at a lower energy of 1.54(11) MeV [4]. Subsequently, Grigorenko and Zhukov showed that the observed peak in the three-body spectrum of the GSI invariant mass measurement could result from the halo nature of the ^{11}Li projectile [2], apparently reconciling the discrepancy between the GSI and Dubna results.

In our experiment we populated ^{10}He in the two-proton and two-neutron removal reaction from a ^{14}Be beam at an energy of 59 MeV/nucleon. This reaction was considered to be more dissipative than the one-proton removal reaction and thus the invariant mass spectrum should not be influenced by the proposed initial state effects. We measured a resonance energy of 1.60(25) MeV [1], consistent with the GSI results [4] but in disagreement with the Dubna data [3].

Earlier this year Sharov *et al.* [5] suggested that our results could be explained by assuming that ^{10}He was populated directly by an α-cluster removal, thus again exhibiting a structure which is due to the halo nature of the initial ^{14}Be. In the present paper, we report a more-detailed analysis of the data to investigate possible evidence for direct cluster removal and search for a resonance in ^{12}He.

II. EXPERIMENTAL METHOD

The experiment was performed at the National Superconducting Cyclotron Laboratory (NSCL) where a 3196 mg/cm^2 ^{9}Be target was bombarded with ^{18}O at 120 MeV/nucleon. The A1900 fragment separator allowed for selection of ^{14}Be from the other fragmentation products as well as the primary beam. The secondary beam then impinged on a 435 mg/cm^2 deuterated polyethylene target at a rate of approximately 1000 pps. The resulting charged fragments were bent by a 4-Tm superconducting sweeper magnet [6] into a collection of position- and energy-sensitive charged-particle detectors, which allowed for element identification of helium via a ΔE-E measurement. Isotope identification of ^{8}He was achieved through correlations between time-of-flight, dispersive angle, and dispersive position of the fragments. This technique is described in further detail in Ref. [7]. The neutrons emitted in-flight traveled undisturbed by the magnetic field towards the Modular Neutron Array (MoNA) [8], which provided a measurement of position and time-of-flight. Together, MoNA and the sweeper system provide a full kinematic measurement of the neutrons and the charged fragment, from which the decay energies of $^{9-12}$He can be calculated. Additional experimental details can be found in Refs. [1,9].

III. ANALYSIS

In the initial analysis [1] only the three-body decay energy spectrum of ^{10}He in coincidence with two neutrons was

*jonesm@nscl.msu.edu
†Present address: TRIUMF, 4004, Wesbrook Mall, Vancouver, British Columbia, Canada V6T 2A3.
‡Present address: LANL, Los Alamos, New Mexico 87545, USA.

calculated. However, a direct two-proton removal reaction would populate ^{12}He, which then would emit four neutrons in-flight in coincidence with ^{8}He. A potential resonance in ^{12}He could be observable in the five-body decay energy spectrum. Thus, we extended our analysis to N-body decay energy spectra for $2 \leqslant N \leqslant 5$ corresponding to the decays of $^{9-12}$He. The N-body decay energy is defined as $E_{\mathrm{decay}} = M_{N\mathrm{body}} - M_{^8\mathrm{He}} - \sum_{i=1}^{i=N-1} m_n$, where $M_{N\mathrm{body}}$ is the invariant mass of the N-body system, $M_{^8\mathrm{He}}$ the mass of ^{8}He, and m_n the mass of a neutron. The invariant mass for an N-body system was calculated from the experimentally measured four-momenta of ^{8}He and the first $N-1$ time-ordered interactions in MoNA.

Due to multiple scattering events in the array, it is necessary to discriminate between true and false multineutron events. For one-neutron events, the contribution from ^{9}He can be enhanced by gating on multiplicity $= 1$ events. In the case of ^{10}He ($2n$ events) separation of scattered events from real two-neutron events was accomplished by applying causality cuts on the relative distance and velocity between the first two interactions in MoNA as described in Ref. [1].

Ideally, similar cuts should be applied to the four-body and five-body decay energy spectra. However, there were insufficient counts for these cuts to be applied. No resonances are apparent in these spectra, which are dominated by multiple scattering events. It was estimated by simulation that the fraction of true four-neutron events in the five-body spectra is approximately 8% below 1 MeV and 3% above 1 MeV.

The large number of free parameters makes it difficult to take all possible population and decay paths for forming ^{8}He from ^{14}Be into account. Thus, the simulations were limited to direct population of ^{12}He and ^{10}He. Three different scenarios, described later, were considered separately for the population of ^{12}He. For ^{10}He the population of the 0^+ ground state and the 2^+ first-excited states were included. The simulations did not distinguish between α removal or $2p2n$ removal. However, a larger contribution to the spectra relative to the ^{12}He population would indicate an α removal because the $2p2n$ removal cross section is expected to be significantly smaller than the $2p$ removal cross section. The different population paths and subsequent decays included in the simulation are shown in Fig. 1.

The removal reactions were modeled with the Goldhaber reaction model in conjunction with a detailed Monte-Carlo package. These simulations included the beam characteristics, the reaction mechanism, and the subsequent decay. Using GEANT4 [10] and MENATE_R [11], the efficiency, resolution, and acceptances of MoNA and the charged particle detectors following the dipole sweeper magnet were incorporated into the simulations, making the results directly comparable to experiment. It has been shown that the inclusion of MENATE_R is important for properly simulating the response of plastic scintillators [12].

The key distinguishing feature between α or $2p2n$ removal and $2p$ removal is the total number of neutrons emitted in each reaction. Hence, it is important to consider both the one and two-neutron decay energy spectra in addition to the multiplicity distribution. This is done by a simultaneous χ^2 minimization procedure on the following six experimental

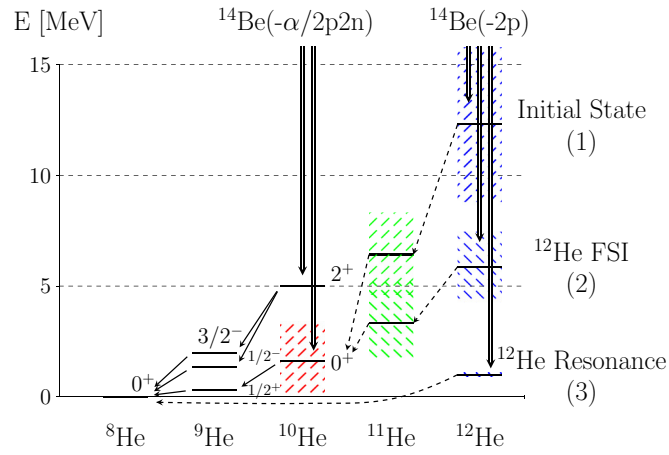

FIG. 1. (Color online) Level scheme for the population and decay of ^{10}He from $\alpha/2p2n$ or $2p$ removal. Hatched areas indicate approximate widths. The different scenarios for populating ^{12}He are described in Sec. III B.

spectra found in Fig. 2: (a) the $^{8}\mathrm{He} + 1n$ decay energy, (b) the multiplicity $= 1$ gated $^{8}\mathrm{He} + 1n$ decay energy, (c) the $^{8}\mathrm{He} + 2n$ decay energy, (d) the decay energy of $^{8}\mathrm{He} + 2n$ gated on multiplicity $= 2$, (e) the $^{8}\mathrm{He} + 2n$ decay energy with the causality cut, and finally (f) the multiplicity distribution.

This simultaneous minimization adds additional constraints to the final fit results compared to fitting the two- and three-body decay energy spectra separately to extract the ^{9}He and ^{10}He resonance parameters, respectively.

A. Direct α or $2p2n$ removal

Due to large uncertainties in ^{10}He and the ^{9}He subsystem, we first consider only direct population of ^{10}He, or $2n$ events. Here we assume that ^{10}He is populated exclusively through α or $2p2n$ removal and that ^{9}He is populated only by sequential decay as shown in Fig. 1. The sequential emission is modeled following the formalism of Volya [13]. We consider both the decay of the ground (0^+) state and the first-excited (2^+) state of ^{10}He through three states in ^{9}He: the $1/2^+$, $1/2^-$, and $3/2^-$ states. The $1/2^-$ state was fixed in energy and width at $E = 1.33$ MeV and $\Gamma = 0.1$ MeV [4]. Additionally, the widths of the $1/2^+$ and $3/2^-$ states were fixed at 8.4 and 0.7 MeV [4,14], respectively, but allowed to vary in energy. For ^{10}He, both states were allowed to vary in energy. However, the width of the 2^+ state was restricted to 1.64 MeV [4]. The range of energies was chosen to encompass a variety of previous measurements [3,4,14–23]. While it is possible to include a decay through the $5/2^+$ state in ^{9}He at energies reported from previous experiments [14,15], this resonance is not well resolved in the data of higher energy and is thus excluded from this analysis. The dominant components needed to describe the data are the decay of the 0^+ state in ^{10}He through the $1/2^+$ state in ^{9}He and the decay of the first-excited 2^+ state though the $1/2^-$ and $3/2^-$ states.

The fitting results with the assumption of α or $2p2n$ removal are shown in Fig. 2. With a χ^2 of 161 for 152 degrees of freedom, the model shows good agreement with the data and

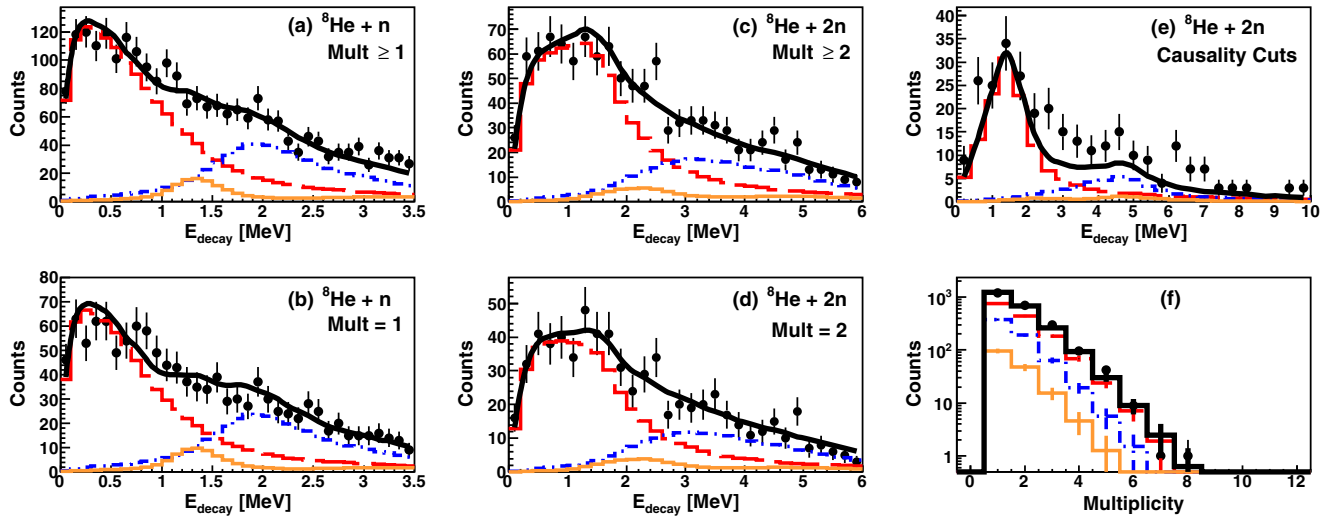

FIG. 2. (Color online) Decay energy spectra assuming $\alpha/2p2n$ removal for (a) $^8\mathrm{He}+1n$, (b) $^8\mathrm{He}+1n$ gated on multiplicity = 1, (c) $^8\mathrm{He}+2n$, (d) $^8\mathrm{He}+2n$ gated on multiplicity = 2, (e) $^8\mathrm{He}+2n$ with causality cuts, and (f) the multiplicity distribution. Measured spectra are indicated by black solid circles. The best fit for α or $2p2n$ removal with no contribution from $2p$ removal is shown as solid black. The fit parameters can be found in Table I. The $l=0$ sequential decay from the 0^+ ground state in ^{10}He is shown by the dashed (red) histogram while the dot-dash (blue) and solid (orange) histograms are decays from the 2^+ state to the $3/2^-$ and $1/2^-$ states in ^{9}He, respectively.

with previous experiments. The resonance parameters for the best fit are summarized in Table I. Only two states differed in energy compared to previous measurements. The $3/2^-$ state in ^{9}He tended to be slightly lower at $1.9^{+0.4}_{-0.2}$ MeV, in contrast to 2.4 MeV [14], and the minimum χ^2 suggests a value of $4.7^{+0.8}_{-0.5}$ MeV for the 2^+ state, compared to 4.0 MeV [4]. It should be mentioned that the fit is insensitive to certain parameters, namely, the scattering length in ^{9}He and, in general, resonance widths. For example, scattering lengths down to -10 fm for the $1/2^+$ state in ^{9}He and widths of the 0^+ state larger than 1 MeV resulted in equally good fits. More importantly, however, the fit demonstrates that it is possible to describe the data entirely with two-neutron events using values in agreement with previous experiments. There is an underprediction of events in the three-body decay energy with causality cuts [panel (e) in Fig. 2], but this discrepancy is not enough to reject the fit when the other histograms are considered. Increasing the widths of the states in ^{10}He or changing their energies affects their shape in the ^{9}He spectra, and the fit presented is the best simultaneous fit. Thus the data do not require significant contributions from direct two-proton removal, which would be expected to have a large cross section compared to α or $2p2n$ removal. However, it is still possible for a component from $2p$ removal to be present up to a limit given by statistical uncertainty.

TABLE I. Resonance parameters for states in ^{9}He and ^{10}He used to fit the $1n$ and $2n$ decay energy spectra. Values with a dagger indicate they were adjusted to best describe the data.

Nucleus	J^π	E (MeV)	Γ (MeV)
^{9}He	$1/2^+$	-3 fm[a] [4]	8.4 [4]
	$1/2^-$	1.33 [4,14]	0.1 [14]
	$3/2^-$	$1.9^{+0.4}_{-0.2}$ †	0.7 [14]
^{10}He	0^+	1.6 [1]	1.8 [1]
	2^+	$4.7^{+0.8}_{-0.5}$ †	1.64[4]

[a]Scattering length for the $l=0$ state.

B. Two-proton removal

To determine any possible contributions from direct population of ^{12}He by two-proton removal we modeled the decay of $^{12}\mathrm{He} \rightarrow {}^8\mathrm{He}+4n$. The three different cases for the population of ^{12}He were (i) a distribution influenced by the initial halo structure of ^{14}Be, henceforth referred to as the ^{14}Be inital-state structure (ISS) [24], (ii) a resonant final-state interaction (^{12}He FSI) [24] peaking at ~6.5 MeV, and (iii) a low-lying resonance described by a Breit-Wigner centered at ~1 MeV. In the ISS and FSI cases, it was assumed that ^{12}He decayed to the 0^+ ^{10}He ground state with a phase-space distribution [25], where the three-body decay energy is determined by the difference between the ^{10}He and ^{12}He decay energy distributions. The remaining ^{10}He then decayed sequentially through ^{9}He following the paths described previously. The third case was modeled as a five-body phase-space breakup decaying directly to ^{8}He. The $2p$-removal decay paths are shown in Fig. 1.

The minimization method described previously was expanded to include two additional spectra to search for a $4n$ component. To enhance the sensitivity to $4n$ events, the raw five-body decay energy spectrum and the five-body decay energy spectrum gated on multiplicity $\geqslant 4$ were analyzed. Although the statistics of these five-body spectra are small and contain very few real four-neutron events they still provide a measure of the amount of scattering in the array. If the reaction were to proceed predominantly by $4n$ emission, the

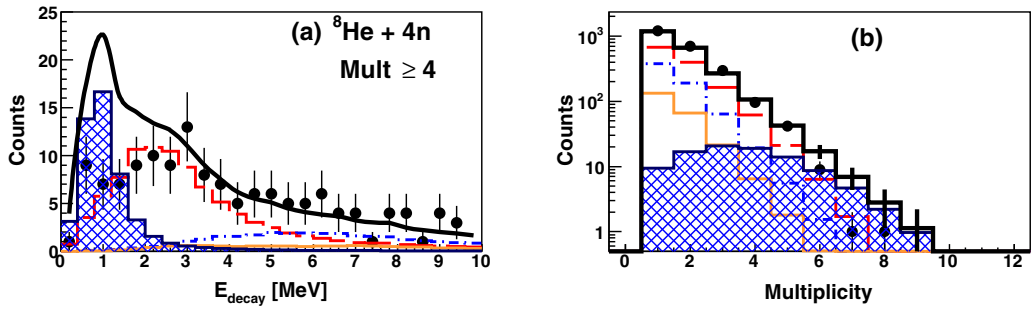

FIG. 3. (Color online) Five-body decay energy spectra for ^{8}He + 4n for all multiplicities (left) and neutron multiplicity distribution (right). The hatched blue histogram is the contribution from a five-body breakup of ^{12}He at $E = 1$ MeV and $\Gamma = 100$ keV with $R(4n/2n) = 1.5\%$. The dash, dot-dashed, and solid lines are the same as those in Fig. 2.

five-body spectra constructed from the first four hits will be enhanced, especially for low-energy neutrons. Combined with the multiplicity distribution, these spectra provide sensitivity to the number of neutrons emitted in the reaction.

In the minimization procedure we start from the α or $2p2n$ description and minimize χ^2 on the same six experimental histograms as before. However, we also track the log-likelihood ratio, Ln [λ], of two five-body spectra, ^{8}He + 4n and ^{8}He + 4n, gated on multiplicity = 4, as well as the multiplicity distribution. The $n\sigma$ confidence intervals are determined by $-\Delta\mathrm{Ln}\,[\lambda] \approx \Delta\chi^2(k)/2$, where $\Delta\chi^2(k)$ is the corresponding deviation from the minimum required to integrate 68%, 95%, and 99% of a χ^2 distribution with k degrees of freedom. Each component of the fit was allowed to vary independently and was treated as a degree of freedom. We chose to track the fit quality of the five-body spectra because they are most sensitive to the presence of a 4n component from $2p$ removal.

We then examine the ratio of 4n to 2n amplitudes, $R(4n/2n)$, or $2p$ to α or $2p2n$ removal cross sections. Taking the minimized parameters from the α or $2p2n$ fit, the amplitude of the $2p$ component is gradually increased while the remaining α or $2p2n$ components are reminimized on the six histograms mentioned earlier. This procedure adjusts $R(4n/2n)$ to best describe the decay energies and relative ratios of events while allowing one to track the increasing deviation from the five-body spectra and the multiplicity.

Overall the best fits achieved for these scenarios are similar to the fits shown in Fig. 2 and are not shown separately. Not surprisingly, because the data can be described with α or $2p2n$ removal alone, the contribution from $2p$ removal in the present fits is small. It should be mentioned that populating ^{10}He from $2p$ removal without any $\alpha/2p2n$ contribution does not describe the data well.

Figure 3 shows the results of a calculation assuming a resonance in ^{12}He at 1 MeV populated with a strength of only 1.5% that of the net α or $2p2n$ components. In the five-body decay energy spectrum [Fig. 3(a)] a large excess of events relative to the data is evident around 1 MeV. At the same time the multiplicity distribution [Fig. 3(b)] is overpredicted for multiplicities beyond 6. Because one would expect the presence of a distinct resonance in ^{12}He to be strongly populated in the $2p$ removal reaction from ^{14}Be, the data do not show evidence of a low-lying state in ^{12}He below 1 MeV.

Even for the other scenarios, which do not assume a distinct resonance in ^{12}He, the upper limit for their population is low. Figure 4 shows the log-likelihood as a function of $R(4n/2n)$ for several cases. In no case does the ratio exceed about 30% and remain within 3σ confidence. The figure demonstrates that the upper limit of $R(4n/2n)$ increases with excitation energy of the five-body system. While the energy for the ^{12}He resonance calculation is at 1 MeV [long-dash-dot (blue) curve] and 4 MeV [short-dash-dot (blue) curve] the mean excitation energies for the FSI calculation [dotted (black) curve] and the ISS calculation (solid curve) are at about 6.5 and 12 MeV, respectively. This increase in the upper limit of $R(4n/2n)$ is predominantly due to the drop-off in efficiency for higher decay energies.

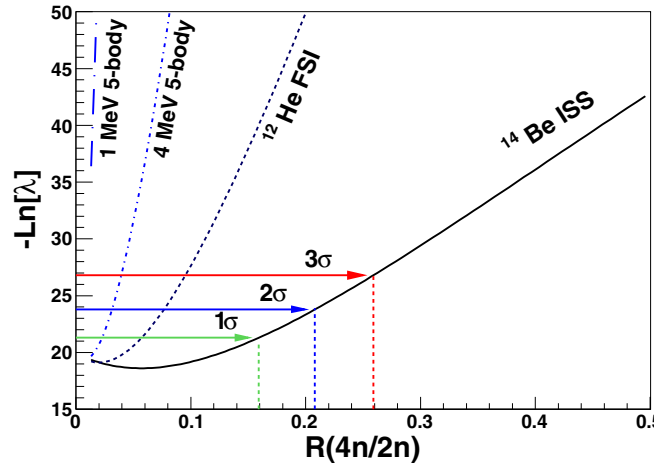

FIG. 4. (Color online) Maximum likelihood for the five-body decay spectra and multiplicity as a function of the ratio of $2p$ to α or $2p2n$ removal $R(4n/2n)$ for several possibilities in the ^{12}He system: a 1-MeV resonance [long-dash-dot (blue) curve], a 4-MeV resonance [short-dash-dot (blue) curve], a ^{12}He FSI calculation [dotted (black) curve], and an ISS calculation (solid curve). The 1σ, 2σ, and 3σ confidence levels are shown by the green, blue, and red arrows, respectively.

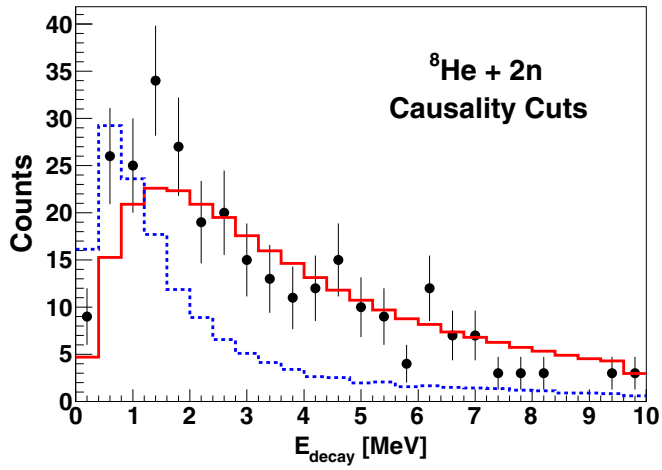

FIG. 5. (Color online) Calculated three-body spectrum with causality cuts for ^{8}He + 2n under the assumption of α removal based on the halo structure of the initial ^{14}Be [solid (red) curve]. The same distribution after folding with experimental resolution, efficiency, and acceptances is shown in the dashed (blue) curve.

IV. DISCUSSION

A small value of $R(4n/2n)$ indicates a direct population of ^{10}He. Because the cross section for $2p2n$ removal is estimated to be at least an order of magnitude smaller than that for the $2p$ removal reaction [26,27] we consider the possibility of α removal. This process was proposed in Ref. [5] to explain our decay energy spectrum. In addition, α removal has also been suggested to explain the population of ^{12}Be from a 55 MeV/nucleon ^{17}C beam incident on a beryllium target [26]. The α-removal three-body distribution for ^{10}He was derived from the same model used to explain the removal from ^{11}Li as presented in Ref. [5]. In this model ^{14}Be is treated as a ^{12}Be core and two neutrons, with the ^{12}Be core considered to be ^{8}He + α. Figure 13 of Ref. [5] showed that such a calculation describes the three-body decay energy from our experiment well. However, the calculations had not been folded with experimental resolutions and efficiencies. The shape of the calculated distribution is significantly changed once the experimental conditions are applied as shown in Fig. 5. The peak of the distribution is shifted towards lower decay energies and the overall width is narrower. Adding a 4n component from the models discussed here does not account for the difference, because the increased 4n contribution overpredicts the multiplicity distribution.

One potential explanation for the small contribution of $2p$ removal events as well as the discrepancy between the data and the direct α-removal model of the three-body decay energy spectrum might be the fact that the charged ^{8}He fragments were not detected at the peak of their momentum distribution. The sweeper magnet was set for lower rigidities so that only the low-energy tail of the overall distribution was recorded. These events probably originate from the more dissipative reactions which could bias the data towards α or $2p2n$ removal relative to $2p$ removal. A similar suppression of the $2p$ removal cross section was observed in the breakup of ^{17}C, where also only the low-energy tail of the momentum distribution was measured [26].

It is possible that the more dissipative reactions could have reduced the effect of the correlation from the ^{14}Be initial state for the direct α removal. In that case then, the observed resonance in ^{10}He should have agreed with the higher value of about 2 MeV previously reported from transfer measurements. Nevertheless, such a dependence of the decay energy spectra on the fragment momentum distribution has not been observed in the past in similar reactions.

In summary, a complete inclusive analysis of multineutron decay energy spectra is a tool to explore neutron unbound systems which decay via the emission of three or four neutrons even if the statistics are not sufficient to extract spectra with clean identification of each neutron. In the present case, no evidence for the existence of a low-lying ($\leqslant$1 MeV) resonance in ^{12}He was found. The three-body decay energy spectrum of ^{10}He could not be described by a reaction mechanism calculation based on the halo structure of the initial ^{14}Be assuming a direct α-particle removal reaction. To distinguish direct α removal from $2p2n$ removal it will be necessary to measure coincident α particles in addition to the charged fragments and the neutrons.

ACKNOWLEDGMENTS

We would like to thank L. V. Grigorenko for thoughtful discussion and for providing theoretical estimates of the five-body decay energies of the ^{12}He system. This work was supported by the National Science Foundation under Grants No. PHY09-22335, No. PHY09-69058, No. PHY09-69173, No. PHY12-05357, No. PHY12-05537, and No. PHY11-02511. The material is also based upon work supported by the Department of Energy National Nuclear Security Administration under Award No. DE-NA0000979.

[1] Z. Kohley *et al.*, Phys. Rev. Lett. **109**, 232501 (2012).
[2] L. V. Grigorenko and M. V. Zhukov, Phys. Rev. C **77**, 034611 (2008).
[3] S. Sidorchuk *et al.*, Phys. Rev. Lett. **108**, 202502 (2012).
[4] H. Johansson *et al.*, Nucl. Phys. A **842**, 15 (2010).
[5] P. G. Sharov, I. A. Egorova, and L. V. Grigorenko, Phys. Rev. C **90**, 024610 (2014).
[6] M. Bird *et al.*, IEEE Trans. Appl. Supercond. **15**, 1252 (2005).
[7] G. Christian *et al.*, Phys. Rev. C **85**, 034327 (2012).
[8] B. Luther *et al.*, Nucl. Instrum. Methods Phys. Res., Sect. A **505**, 33 (2003).
[9] J. Snyder *et al.*, Phys. Rev. C **88**, 031303(R) (2013).
[10] S. Agostinelli *et al.*, Nucl. Instrum. Methods Phys. Res., Sect. A **506**, 240 (2003).
[11] B. Roeder, EURISOL Design Study, Report No. 10-25-2008-006-In-beamvalidations.pdf, pp. 3144, 2008 (unpublished).

[12] Z. Kohley *et al.*, Nucl. Instrum. Methods Phys. Res., Sect. A **682**, 59 (2012).
[13] A. Volya, EPJ Web Conf. **38**, 03003 (2012).
[14] H. Bohlen *et al.*, Prog. Part. Nucl. Phys. **42**, 17 (1999).
[15] T. Al Kalanee *et al.*, Phys. Rev. C **88**, 034301 (2013).
[16] L. Chen *et al.*, Phys. Lett. B **505**, 21 (2001).
[17] K. Seth *et al.*, Phys. Rev. Lett. **58**, 1930 (1987).
[18] K. Seth, Nucl. Phys. A **434**, 287 (1985).
[19] W. von Oertzen *et al.*, Nucl. Phys. A **588**, 129 (1995).
[20] G. Rogachev *et al.*, Phys. Rev. C **67**, 041603 (2003).
[21] M. S. Golovkov *et al.*, Phys. Rev. C **76**, 021605 (2007).
[22] M. S. Golovkov *et al.*, Phys. Lett. B **672**, 22 (2009).
[23] A. Matta *et al.*, RIKEN Accel. Prog. Rep. **45** (2012).
[24] L. V. Grigorenko (private communication).
[25] F. James, Monte Carlo Phase Space, CERN **68-16** (1968).
[26] A. N. Kuchera *et al.*, Phys. Rev. C **91**, 017304 (2015).
[27] J. A. Tostevin (private communication).